



Pyrolysis kinetics and thermodynamic parameters of macroalgae *Cladophora glomerata* based on multi-step devolatilization to assess its bioenergy potential

Zahir Shah¹ · Syed Lal Badshah² · José Luiz Francisco Alves³ · Jean Constantino Gomes da Silva³ · Arshad Iqbal¹

Received: 27 November 2021 / Revised: 4 March 2022 / Accepted: 5 March 2022
© The Author(s), under exclusive licence to Springer-Verlag GmbH Germany, part of Springer Nature 2022

Abstract

Cladophora biomass, through pyrolysis, has great potential for utilization in bioenergy applications and biochar formation. Here, we performed a detailed kinetic and thermodynamic evaluation of the slow pyrolysis of *Cladophora glomerata*. The pyrolysis was performed in a thermogravimetric analyzer using non-oxidative inert conditions of nitrogen gas at a temperature range of 25–800 °C under three low heating rates (5, 10, and 20 °C min⁻¹). In the pyrolysis of *C. glomerata*, three different stages were observed, showing the complex nature of its biomass. The kinetics were obtained through isoconversional methods, where the average activation energies were in the range of 159.5–169.5 kJ mol⁻¹, 221–239 kJ mol⁻¹, and 157–168 kJ mol⁻¹ for stages 1, 2, and 3, respectively, each with a coefficient of determination (R^2) above 0.9. The average values of change in enthalpy (ΔH) were 155.36 kJ mol⁻¹, 217.83 kJ mol⁻¹, and 150.08 kJ mol⁻¹ for stages 1, 2, and 3, respectively, while the average values of change in Gibb's free energy (ΔG) were 169.81 kJ mol⁻¹, 179.90 kJ mol⁻¹, and 273.42 kJ mol⁻¹ for stages 1, 2, and 3, respectively. Thermodynamic analysis of the slow pyrolysis of *C. glomerata* shows that it is an endothermic, non-spontaneous process that proceeds in the direction of producing bioenergy.

Keywords Freshwater macroalgae · Pyrolysis kinetics · Isoconversional methods · *Cladophora glomerata* · Bioenergy potential · Thermodynamic parameters

1 Introduction

Biomass is an alternative source of energy to fossil fuels. The global demand for clean energy has increased in the last 2 years due to natural disasters related to global warming. Although developing countries still depend primarily on fossil fuels, they are also moving toward renewable energy sources. Thermochemical conversion technologies,

including pyrolysis, gasification, hydrothermal carbonization, and combustion, have been proposed as ways to extract bioenergy from algal biomass [1–4]. Pyrolysis, in particular, is considerably better than other thermochemical conversion technologies. This is attributed to its lower emissions, simpler operation, and a reasonable cost [5]. Pyrolysis occurs by supplying heat (high temperatures) to algal biomass, thus converting its organic structure (proteins, carbohydrates, and lipids) into bioenergy products as biochar (solid fraction), pyrolytic gases (non-condensable fraction), and condensable volatiles (bio-oil, liquid fraction) [1, 6]. However, the algae classes differ from one another due to their varying chemical composition. Algae may be modified to obtain a better yield of useful bioenergy by-products such as biochar.

In several pyrolysis techniques applied to algae, samples are either treated with microwaves or with catalysts to improve biofuel production. It has been observed that when *Arthrospira platensis* (*Spirulina platensis*) is pyrolyzed in the presence of a zeolite catalyst, various valuable chemicals such as nitriles, aromatics (benzene, toluene, xylene, etc.), and cyclic hydrocarbons are produced in high yield

✉ Syed Lal Badshah
shahbiochemist@gmail.com

✉ Arshad Iqbal
arshad.iqbal@icp.edu.pk

¹ Department of Botany, Islamia College University Peshawar, Peshawar 25120, Pakistan

² Department of Chemistry, Islamia College University Peshawar, Peshawar 25120, Pakistan

³ Department of Chemical Engineering and Food Engineering, Federal University of Santa Catarina, Florianópolis, Santa Catarina 88040-900, Brazil

[7]. When β -zeolite is used as a catalyst in pyrolysis, the production of light hydrocarbons is high, compared to the oxygenated forms of organic compounds [8]. The pyrolysis of three microalgae, namely, *Scenedesmus almeriensis*, *Nannochloropsis gaditana*, and *Chlorella vulgaris*, has been performed and has yielded several products, as observed through mass spectrometry [9]. Hydrogen gas was produced at 400 °C, along with other useful gases such as carbon monoxide, carbon dioxide, steam, etc. Hydrogen gas and carbon monoxide can be used as fuels. In addition to these gases, a series of light hydrocarbons, alcohols, amines, etc. were also detected [9].

Thus, each pyrolysis method generated different, yet commercially valuable, chemical products. However, if the goal is to produce more biofuel, it is better to use algae that have lower amounts of nitrogen and sulfur to avoid the production of NO_x and SO_x gases. Furthermore, it may be possible to develop a method through which these two types of compounds can be transformed into other products, while the generated biofuel contains only hydrocarbons, hydrogen gas, and carbon monoxide. A fast pyrolysis method has been utilized to determine the energy production values of the marine macroalgae *Enteromorpha prolifera*. The obtained data showed an average heat production capacity of 25.33 MJ kg⁻¹ and 30.27 wt% O₂ [10]. This energy production is quite favorable and showed that the *Enteromorpha* is suitable for bioenergy production.

Due to the high amount of biomass produced by macroalgae, they are an economically favorable source for the preparation of biochar through pyrolysis. For example, Salimi et al. [11] produced olive-shaped magnetic biochar from *Cladophora* biomass through slow pyrolysis using iron as a catalyst [11]. The particles of this biochar have a high surface area of 296.4 m² g⁻¹. Magnetic biochar can be used as an anode material in lithium-ion batteries. This indicates a great potential of macroalgae, since the use of electric cars, which run on lithium ion batteries, is expected to increase in the near future. The suitable pore size of the magnetic biochar of *C. glomerata* makes it an important material for the synthesis of asymmetric super-capacitors when combined with iron oxide [12]. The electrodes of magnetic biochar have a high capacitance and cycling stability, and therefore, it can be used as electric storage device [12]. The biochar obtained from *C. glomerata* also has a high adsorption capacity for heavy metal ions such as chromium, zinc, and copper [13, 14].

There are more than seventy-two thousand and five hundred (72500) species of algae worldwide. *C. glomerata* is a filamentous freshwater macroalga with more than one hundred and eighty-three species all over the world [15]. It exists throughout the world in different freshwater reservoirs. It has a mucilaginous sheath outside its thick wall. Most of the pyrolysis studies so far have been conducted with marine

macroalgae, and very few papers have addressed the pyrolysis of freshwater macroalgae. Furthermore, kinetic studies involving the estimation of thermodynamic parameters for algal biomass pyrolysis are scarce and observed in only a few reports [1, 6, 16].

The novelty of this work relies on the study of the pyrolysis of *C. glomerata*, with a focus on the determination of triplet kinetic and thermodynamic parameters under a multi-stage kinetics point of view. For this, the pyrolysis behavior of *C. glomerata* was first acquired from non-isothermal thermogravimetric measurements. Isoconversional kinetic analysis was applied to thermogravimetric data with concurrent use of four isoconversional methods (Friedman, Flynn–Wall–Ozawa, Kissinger–Akahira–Sunose, and Starink) to determine the activation energy. In addition, compensation effect and master plots were used to determine the pre-exponential factor, and reaction model, respectively. The thermodynamic parameters (ΔH , ΔG , and ΔS) were also determined to obtain a detailed understanding of the pyrolysis of *C. glomerata*. The kinetic and thermodynamic findings from the pyrolysis of *C. glomerata* provide a useful reference for the design of a pyrolytic processing system.

2 Materials and methods

2.1 Collection of algae

The *C. glomerata* was collected from the Swat River and its tributaries in Charsadda city of Khyber Pakhtunkhwa, Pakistan. The collected algae were first washed with tap water for removal of sand and soil debris and then washed thrice with distilled water. The clean algae were placed to dry in the shade. After drying, it was transformed into powder through a home-built grinder. The ground algae were stored in air-tight jars for further use in different experiments.

2.2 Proximate, ultimate, and HHV analyses

The proximate analysis that include their moisture, ash content, volatile carbon, and fixed carbon were determined using the protocol of ASTM D-5142 [17, 18]. For elemental analysis, the EDX technique was used to get an idea about the elemental composition of the sample. The high heating value for *C. glomerata* biomass was obtained using the values from proximate analysis as calculated by earlier works [17–19].

2.3 Thermogravimetric analysis

The thermal pyrolysis of *C. glomerata* was carried out in a thermogravimetric analyzer model TGA Q500 (TA Instruments, New Castle, USA), with a temperature accuracy

of ± 0.1 °C and mass accuracy of $\pm 0.01\%$. A 5.0-mg dried ground *C. glomerata* sample was added to a platinum crucible and was heated from 25 to 800 °C using three different heating rates of 5, 10, and 20 °C min⁻¹, all under a pure nitrogen gas flow of 60 mL min⁻¹. Before each pyrolysis experiment, the whole oven was purged with nitrogen gas to ensure an inert condition. The ICTAC Kinetics Committee recommendations were followed during the experiment [20]. All experiments were performed in triplicate for TGA data reliability.

2.4 Theoretical background for determining the kinetic triplet

The pyrolysis of macroalgae is a complex thermal degradation where larger biopolymers like polysaccharides, proteins, nucleic acids, and lipids are converted into volatile organic compounds that, along with biochar, contain carbon and minerals.

The conversion rate (da/dt) is defined as a product of a temperature-dependent reaction constant and a conversion-dependent reaction model, as given in Eq. (1) [21]:

$$\frac{d\alpha}{dt} = k(T)f(\alpha) \quad (1)$$

where α , t , $k(T)$, and $f(\alpha)$ denote the degree of conversion, the reaction time, the temperature-dependent reaction constant, and the reaction model in the differential form, respectively.

The reaction constant $k(T)$ is dependent on the temperature obeying the Arrhenius' law. Hence, Eq. (2) provides the conversion rate in terms of Arrhenius' law [22]:

$$\frac{d\alpha}{dt} = Ae^{-E_a/RT}f(\alpha) \quad (2)$$

In Eq. (2), A is the pre-exponential factor (min⁻¹), E_a is the activation energy (kJ mol⁻¹), T is the absolute temperature (K), and R is the universal gas constant (8.3145×10^{-3} kJ mol⁻¹ K⁻¹).

Under non-isothermal conditions, where the temperature is a function of time that increases with a constant heating rate ($dT/dt = \beta$), Eq. (2) becomes [23]

$$\frac{d\alpha}{dT} = \frac{A}{\beta} e^{-E_a/RT} f(\alpha) \quad (3)$$

Thus, by integration from Eq. (3), the following equation can be obtained.

$$g(\alpha) = \int_0^1 \frac{d\alpha}{f(\alpha)} = \frac{A}{\beta} \int_{T_0}^T e^{-E_a/RT} dT \equiv \frac{A}{\beta} I(E_a, T) \cong \frac{AE_a}{\beta R} p(x) \quad (4)$$

The most challenging aspect of Eq. (4) is to deduce the dependence of activation energy on the degree of conversion is that this equation has a term " $p(x)$ " ("temperature integral") which cannot be solved directly [1, 24]. Several mathematical approximations have been proposed to reduce the complexity of Eq. (4) for practical calculation of the activation energy.

2.4.1 Determination of the activation energy

In this work, four isoconversional methods were employed to calculate the activation energy: Friedman (Eq. (5)), Flynn–Wall–Ozawa (Eq. (6)), Kissinger–Akahira–Sunose (Eq. (7)), and Starink (Eq. (8)) [25, 26]. The most broadly used integral isoconversional methods are those developed by Flynn–Wall–Ozawa (supported by Doyle's approximation [26]), Kissinger–Akahira–Sunose (supported by Murray and White's approximation [26]), and Starink (supported by Starink's approximation [27]). The results from these different approximations were compared with those from direct differentiation. The Friedman method is the most common differential isoconversional method and is a direct result of applying the natural logarithm to Eq. (3) [21]:

$$\ln\left(\frac{d\alpha}{dt}\right) = \ln\left[\beta\left(\frac{d\alpha}{dT}\right)\right] = \ln[Af(\alpha)] - \frac{E_a}{RT} \quad (5)$$

$$\log \beta = \log\left(\frac{AE_a}{Rg(\alpha)}\right) - 2.315 - 0.4567 \frac{E_a}{RT} \quad (6)$$

$$\ln\left(\frac{\beta}{T^2}\right) = \ln\left(\frac{AR}{E_a g(\alpha)}\right) - \frac{E_a}{RT} \quad (7)$$

$$\ln\left(\frac{\beta}{T^{1.92}}\right) = \text{Constant} - 1.0008 \frac{E_a}{RT} \quad (8)$$

where the values of activation energy (E_a) and their correspondent coefficients of determination (R^2) were calculated by regression lines based on the isoconversional methods of FR [$\ln(da/dt)$ versus $1/T$], FWO [$\log(\beta)$ versus $1/T$], KAS [$\ln(\beta/T^2)$ versus $1/T$], and STK [$\ln(\beta/T^{1.92})$ versus $1/T$]. The intention of employing the four different isoconversional methods is to verify the reliability of the calculations and to confirm the results.

Below, we describe the kinetic compensation effect and integral master-plot methods that were used to estimate the pre-exponential factor and a probable reaction model of the pyrolysis of the *C. glomerata*. Both methods apply theoretical reaction mechanism models for deducing the pre-exponential factor and the probable reaction model. In Table S1 (in the Supplementary Material), seventeen classical reaction models (in both differential and integral forms)

commonly adopted to represent the non-isothermal kinetic characteristics of solid-state reactions are presented, which comprise different reaction mechanisms, such as power-law (P-type), Avrami-Erofeev (A-type), reaction order (F-type), geometrical contraction (R-type), and diffusion (D-type) [28, 29].

2.4.2 Determination of the pre-exponential factor

It is accepted that for thermally induced reactions in solids like biomass pyrolysis, the natural logarithm of the pre-exponential factor ($\ln A$) should follow a linear relationship with the activation energy (E_a). This functional phenomenon is mathematically based on the linear relationship defined in Eq. (9) [5].

$$\ln(A)_i = a_i \cdot E_{ai} + b_i \quad (9)$$

where a and b are constants often referred to as the compensation coefficients, and the subscript “ i ” stands for each of the candidate reaction models $g(\alpha)$ tested to represent the pyrolysis process (listed in Table S1). With the straight line obtained by plotting $\ln A$ against E_a taking into account different reaction models, it is possible to obtain the compensation coefficients a (slope) and b (y-intercept), which allows for further estimation of the pre-exponential factor.

2.4.3 Determination of the reaction model

The integral master-plot method aims to figure out the probable reaction model involved in the pyrolysis reaction. The degree of conversion equal to 50% was taken as a reference value ($\alpha=0.5$), and then experimental kinetic curves were normalized into experimental master plot curves. After this, a comparison of the theoretical master plot curves [$(g(\alpha)/g(0.5))$ versus α], done by assuming different candidate reaction models (listed in Table S1) with the experimental master plot curves [$(p(x)/p(\times 0.5))$ versus α], allows selection of the probable reaction model. The classical expression of the integral master plot method is given by Eq. (10) [28]:

$$\frac{g(\alpha)}{g(0.5)} = \frac{p(x)}{p(x_{0.5})} \quad (10)$$

where $g(0.5)$ is the reaction model under its integral form at the reference conversion ($\alpha=0.5$) and $p(x_{0.5})$ is the approximate function with $x = E_a/RT_{0.5}$.

2.4.4 Comparison of statistical metrics

Statistical analysis was devoted to comparing simulation results with experimental data to verify the kinetic results acquired. The coefficient of determination (R^2) as given in

Eq. (11) [30], quality of fit (QOF) as given in Eq. (12) [31], and residual sum of squares (RSS) as given in Eq. (13) [28] were used to verify the consistency between reconstructed and experimental kinetic curves:

$$R^2 = 1 - \frac{\sum \left[\left(\frac{d\alpha}{dt} \right)_{\text{exp}} - \left(\frac{d\alpha}{dt} \right)_{\text{sim}} \right]^2}{\sum \left[\left(\frac{d\alpha}{dt} \right)_{\text{exp}} - \left(\frac{d\alpha}{dt} \right)_{\text{average}} \right]^2} \quad (11)$$

$$QOF(\%) = \left(1 - \frac{\sqrt{\sum \left[\left(\frac{d\alpha}{dt} \right)_{\text{exp}} - \left(\frac{d\alpha}{dt} \right)_{\text{sim}} \right]^2 / N}}{\left[\left(\frac{d\alpha}{dt} \right)_{\text{exp}} \right]_{\text{max}}} \right) \cdot 100 \quad (12)$$

$$RSS = \sum \left[\left(\frac{d\alpha}{dt} \right)_{\text{exp}} - \left(\frac{d\alpha}{dt} \right)_{\text{sim}} \right]^2 \quad (13)$$

where $(d\alpha/dt)_{\text{exp}}$ is the values of conversion rate experimentally measured, $[(d\alpha/dt)_{\text{exp}}]_{\text{max}}$ is the maximum value of conversion rate experimentally measured, $(d\alpha/dt)_{\text{average}}$ is the average value of conversion rate experimentally measured, $(d\alpha/dt)_{\text{sim}}$ is the values of conversion rate numerically calculated by using classical Runge–Kutta 4th-order method, and N is the total number of experimental determinations used in the simulations.

2.5 Estimation of thermodynamic parameters

A study of the biomass pyrolysis thermodynamic parameters provides valuable knowledge about its feasibility and energy requirements [32, 33]. In this study, pyrolysis of *C. glomerata* was thermodynamically characterized in terms of enthalpy changes (ΔH), Gibb's free energy changes (ΔG) and entropy changes (ΔS), which can be estimated by Eqs. (14), (15), and (16), respectively [33–35]:

$$\Delta H = E_a + R \cdot T \quad (14)$$

$$\Delta G = E_a + R \cdot T_m \cdot \ln \left(\frac{k_B \cdot T_m}{h \cdot A} \right) \quad (15)$$

$$\Delta S = \frac{\Delta H - \Delta G}{T_m} \quad (16)$$

where k_B is the Boltzmann constant ($1.381 \times 10^{-23} \text{ J K}^{-1}$), h is the Plank constant ($6.626 \times 10^{-34} \text{ J s}^{-1}$), and T_m is the peak temperature (K) related to the maximum mass loss in DTG curves.

3 Results and discussion

3.1 Proximate, ultimate, and high heating value analysis

Table 1 reports the typical physicochemical characterization of shade dried *C. glomerata*, including proximate analysis, ultimate analysis, and heating values that were measured and compared with the ones from the literature data [17, 36, 37]. The data from EDX is presented in Figure S1.

3.2 Pyrolysis behavior from thermogravimetric analysis

The thermogravimetric curves (TGs) and first-order derivative of thermogravimetric curves (DTGs) with respect to temperature for *C. glomerata* are shown in Fig. 1. The initial mass loss of temperatures under 150 °C (4.64 ± 0.40 wt.%) is ascribed to the evaporation of inherent moisture [17]. An induction section takes place within a temperature interval of 150 to 220 °C, which is related to the slow decomposition process of low molecular weight hydrocarbons. The mass loss detected in temperatures below 220 °C was disregarded for kinetic evaluation.

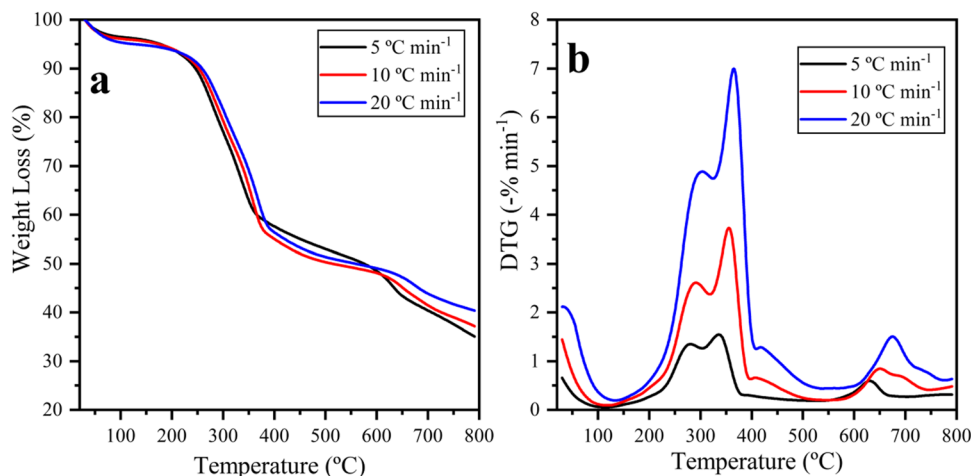
Table 1 Physicochemical characterization of *C. glomerata*, including proximate analysis, ultimate analysis, and heating values

<i>C. glomerata</i>	This Work	Gao et al. [36]	Plis et al. [17]	Norouzi et al. [37]
<i>Proximate analysis</i> (wt.%)				
Moisture	6.0	Not provided	9.10 ^b	4.50 ^b
Volatile matter	50.0	Not provided	48.64 ^b	46.30 ^b
Fixed carbon	4.0	Not provided	5.76 ^b	14.70 ^b
Ash	40.0	21.90 ^a	36.50 ^b	34.50 ^b
<i>Ultimate analysis</i> (wt.%)				
Carbon	33.86	37.00 ^a	26.80 ^b	34.40 ^b
Hydrogen	Not provided	3.60 ^a	3.53 ^b	5.00 ^b
Nitrogen	2.24	4.70 ^a	2.14 ^b	5.20 ^b
Sulfur	2.32	2.40 ^a	0.22 ^b	2.30 ^b
Oxygen	49.07	30.40 ^a	30.81 ^b	18.60 ^b
<i>Chemical composition</i> (wt.%)				
Carbohydrates	Not provided	25.10 ^a	Not provided	32.40 ^b
Lipids	Not provided	8.70 ^a	Not provided	5.30 ^b
Proteins	Not provided	29.50 ^a	Not provided	27.80 ^b
<i>Heating values</i> (MJ kg ⁻¹)				
HHV	15.06	Not provided	10.29 ^b	14.97 ^b
LHV	Not provided	Not provided	9.30 ^b	Not provided

^aDry basis

^bAir-dried basis

Fig. 1 **a** Thermogravimetric curves and **b** first derivative thermogravimetric curves with increasing temperature for the pyrolysis of *C. glomerata* recorded at different heating rates



The second region (around 220–400 °C) presents the major mass loss of about 36.57 ± 0.98 wt.%, which corresponds to the thermal decomposition of different biopolymer fractions present in *C. glomerata*, and this mass loss region is classified as the active pyrolysis region. In the active pyrolysis region, the first noticeable peak is often assigned to the thermal decomposition of carbohydrates, while the second noticeable peak can be ascribed to the thermal decomposition of proteins. Thus, the pyrolysis behavior of *C. glomerata* is in agreement with the well-known fact from the literature that thermal decomposition of carbohydrates occurs from 200 to 300 °C; thermal decomposition of proteins proceeds from 300 to 390 °C [1, 38, 39]. The mass loss under a temperature higher than 500 °C was assigned to the thermal decomposition of inorganic matter and, to some extent, by formed biochar [17, 36], and this mass loss region is categorized as the passive pyrolysis region. Several studies dealing with the pyrolysis of macroalgae biomass reported the occurrence of thermal decomposition of inorganic matter at a high-temperature region [1, 38, 40].

The remaining mass after the pyrolysis of *C. glomerata* is directly related to the total content of fixed carbon and ash, which is also an indication of the biochar yield. At 800 °C, the mass of *C. glomerata* remained close to 37.53 ± 1.90 wt %, which agrees with the proximate analysis reported by Plis et al. [17]. As displayed in Fig. 1b, the pyrolytic behavior of the *C. glomerata* with increasing heating rate tended to shift toward higher temperatures. For illustration, the position of the maximum peak is shifted from 337 °C (at 5 °C min⁻¹) to 365 °C (at 20 °C min⁻¹). This phenomenon can be explained by the thermal lag that is expected to promote a slowdown in the pyrolytic behavior at higher heating rates. The reason for this is that the rising heating rate decreases the characteristic time for devolatilization of lignocellulosic structure which leads to a less effective heat transfer [33, 41].

Based on TG/DTG curves, the temperature region within 220–750 °C was selected for the kinetic evaluation. This temperature region was divided into three successive stages: the first and second stages, which comprise the active pyrolysis zone, represent the thermal decomposition of carbohydrates and proteins, respectively; and the last stage (around

600–750 °C), which is located in the passive pyrolysis zone, represents the thermal decomposition of inorganic matter.

3.3 Kinetic triplet examination

Four isoconversional methods (FR, FWO, KAS, and STK), the compensation effect method, and the master plots method were applied to the TGA data of *C. glomerata* under an inert atmosphere to calculate the kinetic triplet, which encompasses the activation energy, the pre-exponential factor, and the reaction model.

3.3.1 Activation energy from isoconversional methods

Using the three heating rates of 5, 10 and 20 °C min⁻¹, the dependence of activation energy with the degree of conversion was elucidated through four isoconversional methods in the conversion range of 0.05–0.95, with an increment of 0.05. The average values of activation energy obtained from the isoconversional methods of FR, FWO, KAS, and STK for each kinetic stage of the *C. glomerata* pyrolysis are presented in Table 2, along with their coefficients of determination.

Note from Table 2 that the activation energy values estimated by the differential method of FR are greater than the ones computed by the integral methods of FWO, KAS, and STK. According to the literature [42, 43], the numerical differentiation involved in the FR method implies imprecise and inaccurate activation energy values, because it is more sensitive to experimental noises. Also, the coefficients of determination for FR, FWO, KAS, and STK methods are greater than 0.898, indicating the applicability of these isoconversional methods to calculate the activation energy. The values of activation energy and coefficient of determination at different degrees of conversion were obtained by the four isoconversional methods for each of the devolatilization stages during the pyrolysis of *C. glomerata* are provided as in Table S2 (Supplementary Material).

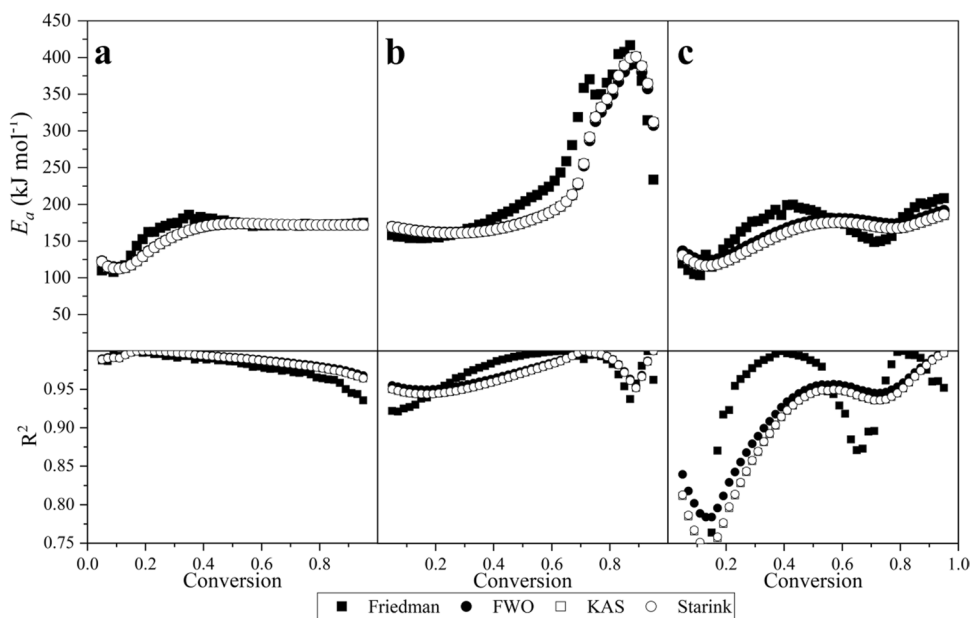
Figure 2 shows the dependence of the activation energy on the degree of conversion as determined by the isoconversional methods of FR, FWO, KAS, and STK for pyrolysis of *C. glomerata*, assuming three successive kinetic stages. In

Table 2 Average values of activation energy and their coefficients of determination computed using the isoconversional methods of FR, FWO, KAS, and STK for pyrolysis of *C. glomerata*, assuming three kinetic stages

Isoconversional method	First stage		Second stage		Third stage	
	E_a (kJ mol ⁻¹)	R^2	E_a (kJ mol ⁻¹)	R^2	E_a (kJ mol ⁻¹)	R^2
FR	169.49	0.9808	239.25	0.9744	168.26	0.9253
FWO	159.72	0.9892	221.43	0.9711	163.03	0.9145
KAS	159.01	0.9880	222.30	0.9679	156.44	0.8989
STK	159.50	0.9881	222.90	0.9681	157.17	0.8996

Average results (E_a and R^2) were estimated in the conversion range of 0.05–0.95 with an increment of 0.001

Fig. 2 Dependence of the activation energy on the degree of conversion using different isoconversional methods, FR, FWO, KAS, and STK, during the pyrolysis of *C. glomerata*, considering three successive kinetic stages: **a** first pyrolysis stage (220–300 °C), **b** second pyrolysis stage (300–400 °C), and **c** third pyrolysis stage (600–750 °C)



short, the different applied isoconversional methods provide almost the same values, except for the FR method which provides the same dependency, but with a small overestimation of values of activation energy.

Considering the first pyrolysis stage, the average activation energies, calculated by the FWO, KAS, and STK integral methods, were 159.72, 159.01, and 159.50 kJ mol^{-1} , respectively, and when calculated by the FR differential method, it was 169.49 kJ mol^{-1} (Table 2). As illustrated in Fig. 2a, the activation energy initially decreased from 119.19 ± 4.59 kJ mol^{-1} (when $\alpha = 0.05$) to 112.94 ± 0.97 kJ mol^{-1} (when $\alpha = 0.10$), and then progressively increased to 173.81 ± 2.04 kJ mol^{-1} (when $\alpha = 0.45$). After $\alpha = 0.45$, the activation energy is practically independent of the degree of conversion. This is observed until $\alpha = 0.95$ is reached.

In the case of the second pyrolysis stage, the average activation energies, computed by the FWO, KAS, and STK integral methods, were 221.43, 222.30, and 222.90 kJ mol^{-1} , respectively, and when computed by the FR differential method, it was 239.25 kJ mol^{-1} (Table 2). As displayed in Fig. 2b, the activation energy initially decreased from 169.42 ± 0.34 kJ mol^{-1} (when $\alpha = 0.05$) to 160.89 ± 0.69 kJ mol^{-1} (when $\alpha = 0.25$), and then progressively increased to 190.65 ± 0.65 kJ mol^{-1} (when $\alpha = 0.60$), as determined by the FWO, KAS, and STK integral methods. After $\alpha = 0.60$, the activation energy abruptly increased to 395.13 ± 3.83 kJ mol^{-1} (when $\alpha = 0.90$) and finally decreased to 314.21 ± 1.81 kJ mol^{-1} (when $\alpha = 0.95$). Peculiarly, with regard to the FR differential method, the activation energy initially decreased from 158.27 kJ mol^{-1} ($\alpha = 0.05$) to 153.95 kJ mol^{-1} ($\alpha = 0.15$), and then linearly increased to 228.33 kJ mol^{-1} ($\alpha = 0.60$). After $\alpha = 0.60$, the activation

energy abruptly increased to 405.12 kJ mol^{-1} ($\alpha = 0.85$) and finally decreased to 238.10 kJ mol^{-1} ($\alpha = 0.95$). As previously presumed, the second pyrolysis stage is predominantly governed by the thermal decomposition of proteins. Expressly, the second pyrolysis stage displayed the highest values of activation energy, typifying a high energy requirement to decompose proteins in *C. glomerata*.

With regard to the third pyrolysis stage, the average activation energies, estimated using the FWO, KAS, and STK integral methods, were 163.03, 156.44, and 157.17 kJ mol^{-1} , respectively, The FR differential method, however, provided an estimation of 168.26 kJ mol^{-1} for the average activation energy (Table 2). As presented in Fig. 2c, the activation energy initially decreased from 132.30 ± 2.68 kJ mol^{-1} ($\alpha = 0.05$) to 119.03 ± 3.23 kJ mol^{-1} ($\alpha = 0.15$), and then progressively increased to 176.98 ± 2.49 kJ mol^{-1} ($\alpha = 0.60$), as determined by the FWO, KAS, and STK integral methods. After $\alpha = 0.60$, the activation energy gradually decreased to 169.85 ± 2.81 kJ mol^{-1} ($\alpha = 0.80$) and finally increased to 187.74 ± 2.62 kJ mol^{-1} ($\alpha = 0.95$). Specifically, regarding the FR differential method, the activation energy initially decreased from 119.73 kJ mol^{-1} ($\alpha = 0.05$) to 114.35 kJ mol^{-1} ($\alpha = 0.10$), and then progressively increased to 196.53 kJ mol^{-1} ($\alpha = 0.40$). After $\alpha = 0.40$, the activation energy gradually decreased to 151.95 kJ mol^{-1} ($\alpha = 0.75$) and finally increased to 207.89 kJ mol^{-1} (when $\alpha = 0.95$). This behavior demonstrates the complexity involved in the pyrolysis of *C. glomerata* at a high-temperature region. The average value of the coefficient of determination for the third kinetic stages varies from 0.898 to 0.925, although satisfactory, indicates a higher dispersion of the TGA data, which is explained by the possible occurrence of multiple and complex reactions during the thermal decomposition of

inorganic matter. In a previous work dealing with the pyrolysis of the freshwater macroalgae *Spirogyra crassa* [38], similar values of the coefficient of determination were found in the thermal decomposition of inorganic matter, which are corroborating with these particular results.

Gao et al. [36] evaluated the activation energy for the pyrolysis of macroalgae *C. glomerata*, based on a single-step kinetic analysis, which was estimated from the KAS and FR methods as being in the ranges of 150.31–303.01 kJ mol⁻¹ and 148.70–318.61 kJ mol⁻¹, respectively. Thus, the average activation energies acquired for pyrolysis of *C. glomerata*, in this study, agree with the results reported in the literature. From the kinetic viewpoint, higher values of activation energy imply that the pyrolytic conversion is unfavorable due to a considerable activation barrier. Thus, pyrolysis of *C. glomerata* (with average activation energy within a range of 156.4–239.3 kJ mol⁻¹) seems to be kinetically more attractive than sub-bituminous coal (average value of 338 kJ mol⁻¹) [44] and coffee silverskin (average value in a range of 268–285 kJ mol⁻¹) [45].

Among the four isoconversional methods, the Starink method is expected to provide a more accurate estimate of the activation energy [27, 46]. Thus, average values of activation energy acquired using the STK method were chosen for further determination of the pre-exponential factors and thermodynamic parameters.

3.3.2 Compensation effect method for determining the pre-exponential factor

Figure 3 presents the straight-line graphs of the natural logarithm of the pre-exponential factor ($\ln A$) versus activation

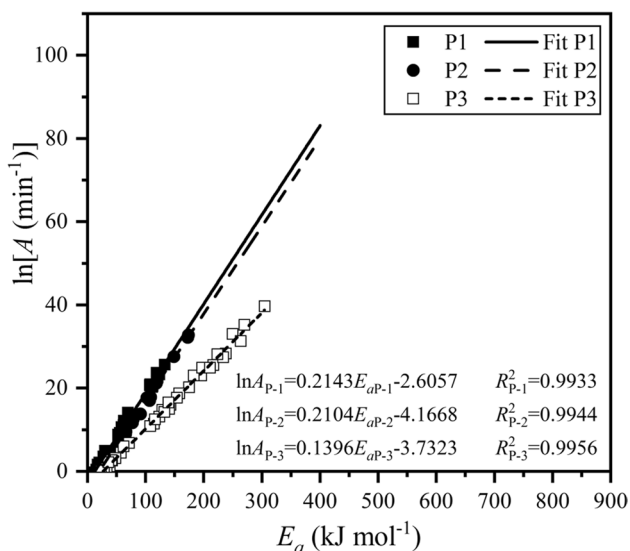


Fig. 3 Straight-line plots between the pre-exponential factor at natural logarithmic form ($\ln A$) and the activation energy (E_a) for each pyrolysis stage of *C. glomerata*

energy (E_a values from the STK method), with high coefficients of determination ($R^2 \geq 0.993$). The pre-exponential factors of each devolatilization stage derived from the pyrolysis of macroalgae *C. glomerata* were estimated to be $5.16 \times 10^{13} \text{ min}^{-1}$ (for P-1), $3.65 \times 10^{18} \text{ min}^{-1}$ (for P-2), and $8.14 \times 10^7 \text{ min}^{-1}$ (for P-3). These orders of magnitude agree closely with the ones found in the related literature. For instance, Shahid et al. [16] reported pre-exponential factors with orders of magnitude in the range of 10^{10} – 10^{20} min^{-1} for the pyrolysis of residual microalgal biomass. Vasudev et al. [6] reported a pre-exponential factor with an order of magnitude between 10^9 min^{-1} and 10^{24} min^{-1} for the pyrolysis of microalgal biomass (*Spirulina*).

The wide range in the order of magnitude of the pre-exponential factors (between 10^7 and 10^{18} min^{-1}) can be attributed to the complex composition of *C. glomerata*. This trend agrees with observations previously reported in the literature for microalgal biomass [16]. With respect to the order of magnitude of the pre-exponential factor, some kinetic studies on lignocellulosic biomass pyrolysis suggested a surface reaction for an order of magnitude below 10^9 min^{-1} , and a simpler chemistry pathway for an order of magnitude of 10^9 min^{-1} or higher [34, 47]. Thus, for pyrolysis of *C. glomerata*, the first and second kinetic stages are assigned to simpler chemistry reactions, while the third kinetic stage corresponds to a surface reaction.

3.3.3 Evaluating the most probable reaction model

The overlap of the theoretical and experimental master plot curves was adopted to find the most probable reaction model

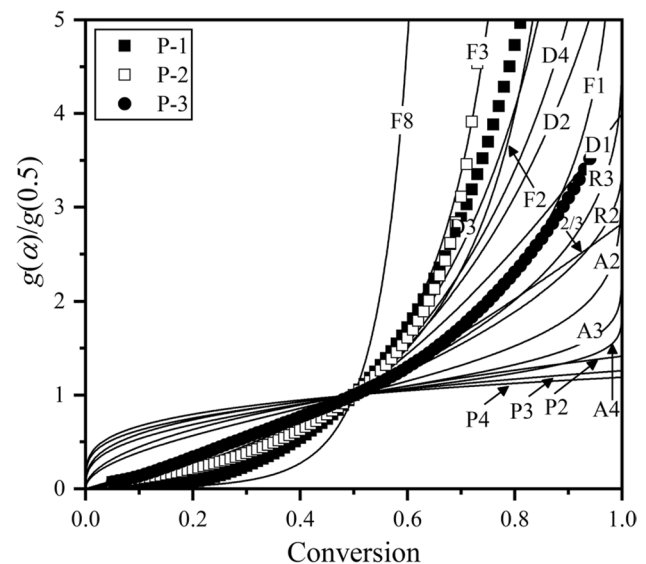


Fig. 4 Overlap of the theoretical and experimental master plot curves [$g(\alpha)/g(0.5)$ versus α] for each pyrolysis stage of *C. glomerata*

of the different pyrolysis stages of *C. glomerata* (refer to Fig. 4), where the reaction model with the lowest relative error was selected as the suitable reaction mechanism for the pyrolysis process.

The relative errors between the theoretical and calculated master plot curves are given in Table 3, showing that the probable reaction model of the first pyrolysis stage is D3 (three-dimensional diffusion–reaction model), with differential form $D3 = 3/2(1 - \alpha)^{2/3}[1 - (1 - \alpha)^{1/3}]^{-1}$. In diffusion-controlled reactions, the conversion rate is controlled by the diffusion of volatile products, where the D3 model assumes a diffusion-controlled reaction involving spherical particles.

Concerning the second pyrolysis stage (P-2), the lowest relative error ($\epsilon = 0.78\%$) was obtained for F3 (third-order reaction model), with differential form $F3 = (1 - \alpha)^3$. The third pyrolysis stage (P-3) corresponds closely to the first-order reaction model, with differential form $F1 = (1 - \alpha)$, which presented the lowest relative error ($\epsilon = 0.07\%$). In particular, the second and third pyrolysis stages are derived

from the chemical kinetics with a conversion rate based on the reaction order, i.e., the conversion rate is proportional to the concentration of reactant raised to a particular exponent “*n*” [1]. Literature findings concerning the pyrolysis of algal biomass also tend toward diffusion–reaction models together with reaction order–based models [6, 25].

3.3.4 Reproducing the experimental pyrolysis behavior

Although isoconversional methods, compensation effect method, and master plot method provide accurate estimations of the kinetic triplets, their practical applicability requires an additional verification step, by demonstrating that the computed kinetic triplets could reproduce satisfactorily the experimental mass-loss curves used in kinetic computations. For this purpose, the three kinetic triplets computed were combined in Eq. 17 to provide an overall kinetic expression that describes the multi-step pyrolytic behavior of *C. glomerata*.

$$\frac{d\alpha}{dt} = \eta_1 5.16 \times 10^{13} e^{-159499/RT} 3/2(1 - \alpha)^{2/3} [1 - (1 - \alpha)^{1/3}]^{-1} + \eta_2 3.65 \times 10^{18} e^{-222903/RT} (1 - \alpha)^3 + \eta_3 8.14 \times 10^7 e^{-157169/RT} (1 - \alpha) \tag{17}$$

Table 3 Relative error calculated from the relation between theoretical and calculated master plot curves for each pyrolysis stage of *C. glomerata*

Model	<i>f</i> (α)	Relative error (%)		
		P-1	P-2	P-3
P2	$2\alpha^{1/2}$	1.3099	26.8095	0.5606
P3	$3\alpha^{2/3}$	1.4345	29.6541	0.6436
P4	$4\alpha^{3/4}$	1.5003	31.1856	0.6859
P2/3	$2/3\alpha^{-1/2}$	0.7065	14.5334	0.1142
A2	$2(1 - \alpha)[-\ln(1 - \alpha)]^{1/2}$	1.0336	19.1382	0.4033
A3	$3(1 - \alpha)[-\ln(1 - \alpha)]^{2/3}$	1.2261	23.6772	0.5280
A4	$4(1 - \alpha)[-\ln(1 - \alpha)]^{3/4}$	1.3338	26.3368	0.5945
F1	$1 - \alpha$	0.5924	10.0656	0.0692
F2	$(1 - \alpha)^2$	0.3036	3.2866	0.2034
F3	$(1 - \alpha)^3$	0.3427	0.7767	0.4263
F8	$(1 - \alpha)^8$	1.0566	2.7877	3.3078
R2	$2(1 - \alpha)^{1/2}$	0.7906	14.9044	0.1899
R3	$3(1 - \alpha)^{2/3}$	0.7242	13.2463	0.1469
D1	$1/2\alpha^{-1}$	0.4570	10.8747	0.3965
D2	$[-\ln(1 - \alpha)]^{-1}$	0.3035	8.0196	0.5575
D3	$3/2(1 - \alpha)^{2/3}[1 - (1 - \alpha)^{1/3}]^{-1}$	0.1373	5.1728	0.7716
D4	$3[2((1 - \alpha)^{-1/3} - 1)]^{-1}$	0.2444	6.9364	0.6282

“ η ” is the average mass loss fraction for each distinct pyrolysis stage, resulting in 0.332, 0.482, and 0.186 for the first, second, and third pyrolysis stages, respectively. The Runge–Kutta 4th-order method was used for solving the overall kinetic expression (Eq. 17).

A comparison between the simulated and experimental pyrolysis behavior (in the form of *da/dt*) with respect to temperature is shown in Fig. 5.

The simulated pyrolysis behavior shows good agreement with the experimental pyrolysis behavior, with a coefficient of correlation in the range 0.728–0.944, *RSS* values lower than 0.05, and a satisfactory quality of fit (*QOF* > 86.3%). The overall kinetic expression (Eq. 17) satisfactorily described the complexity of the pyrolysis of *C. glomerata*, proving its relevance for design and scale-up purposes.

Gao et al. [36] estimated the activation energy of the pyrolysis of *C. glomerata* using the isoconversional methods of KAS and FR and determined the pre-exponential factor and reaction order by the Coats-Redfern method. The referred authors reported that activation energy varies between 150.31 and 303.01 kJ mol⁻¹ and between 148.70 and 318.61 kJ mol⁻¹ for KAS and FR methods, respectively. From the Coats-Redfern method, the pre-exponential factor and reaction order for the pyrolysis of *C. glomerata* presented values ranging from 1.33×10^{28} to 7.56×10^{28} min⁻¹

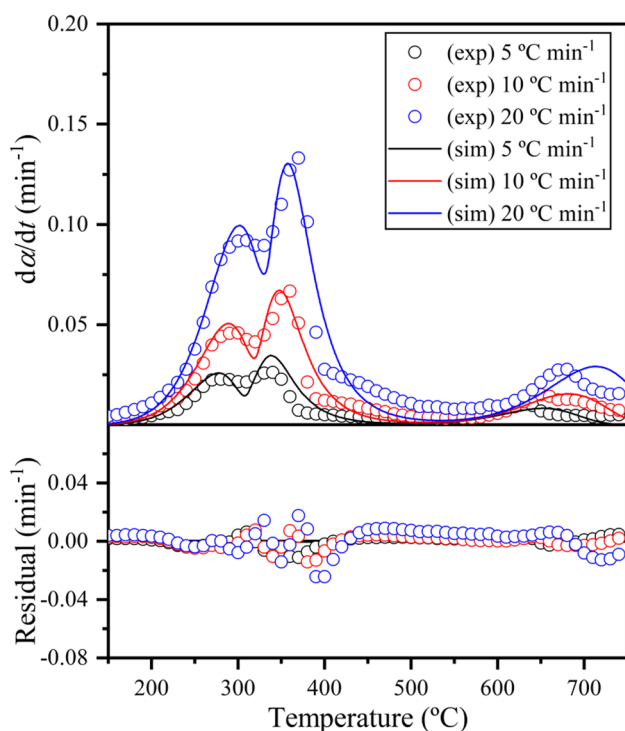


Fig. 5 Comparison between the simulated (symbols) and experimental (lines) pyrolysis behaviors of *C. glomerata* recorded at 5, 10, and 20 °C min⁻¹

and from 7.3 to 9.8, respectively. Plis et al. [17] modeled the pyrolysis behavior of *C. glomerata* as three independent parallel reactions. Based on this assumption, the referred authors reported that the first reaction, ascribed to the hemicellulose decomposition, occurred with an activation energy of 32 kJ mol⁻¹; the second reaction, ascribed to the decomposition of cellulosic and ligneous material, occurred with an activation energy of 177 kJ mol⁻¹; and the third reaction, ascribed to the decomposition of the mineral content and final carbonaceous material, occurred with an activation energy of 48 kJ mol⁻¹. Differences in kinetic triplets are justified by different methodologies employed in the literature studies mentioned for comparison purposes. The present work contributed to the current state of the art, by exposing a comprehensive kinetic study of the pyrolysis of *C. glomerata* in terms of kinetic triplet under a multi-stage approach, with the confirmation of the acquired kinetic triplet results using statistical metrics. Only the values of activation energy estimated in the present work exhibit certain similarities to those reported by Gao et al. [36], both of which use the iso-conversional methods for estimating the values of activation energy. It should be underscored that the kinetic methodologies used in this study for computing the kinetic triplets are aligned with recent recommendations provided by the ICTAC Kinetics Committee recommendations for the analysis of multi-step kinetics [48].

3.4 Thermodynamics results

The thermodynamic analysis was carried out to evaluate the enthalpy changes (ΔH), Gibb's free energy changes (ΔG) and entropy changes (ΔS), which are important parameters for interpreting the feasibility and energy requirements of biomass conversion into biofuel via pyrolysis [32, 33]. As the pyrolysis of *C. glomerata* was assumed to contain three separate pyrolysis stages, the thermodynamic parameters with respect to the degree of conversion were determined separately for each pyrolysis stage, as listed in Table 4.

The values of ΔH for the pyrolysis of *C. glomerata* ranged from 149.03 to 217.96 kJ mol⁻¹, presenting average values of 155.36 ± 0.15 kJ mol⁻¹ for the first stage, 217.83 ± 0.12 kJ mol⁻¹ for the second stage, and 150.08 ± 0.18 kJ mol⁻¹ for the third stage. Considering the positive ΔH values, it can be inferred that the pyrolytic conversion of *C. glomerata* into biochar, bio-oil, and pyrolytic syngas has a heat-absorbing nature (i.e., endothermic reaction). The values of ΔH for the pyrolysis of *C. glomerata* are lower than the ones found for sub-bituminous coal (> 250 kJ mol⁻¹) [49] and comparable with macroalgal biomass (142.7–244.2 kJ mol⁻¹) [1]. Reduced ΔH values imply lower energy requirements, which is an advantage of *C. glomerata* for bioenergy production over low-rank coals.

The difference between the values calculated for E_a and ΔH can be associated with the “potential energy barrier”, and if this difference is below 8 kJ mol⁻¹, an energy-efficient conversion for bioenergy production is expected [50]. Thus, with $E_a - \Delta H$ values below 7.1 kJ mol⁻¹, the pyrolysis of *C. glomerata* tends to be favorable toward bioenergy production due to its low potential energy barrier.

The magnitude of the ΔG parameter quantifies the favorability of biomass conversion into biofuel via pyrolysis. When the magnitude of ΔG is high, a lower favorability for pyrolytic conversion is expected [51]. Positive values of ΔG for pyrolysis of *C. glomerata* ranged from 168.71 to 291.70 kJ mol⁻¹, which match closely with the range of values reported for marine macroalgal biomass (146.9–304.5 kJ mol⁻¹) [1] and lignocellulosic biomass (158.3–212.1 kJ mol⁻¹) [52]. Thus, it is possible to infer that favorability for pyrolysis of *C. glomerata* is acceptable. The positive signs of both ΔH and ΔG indicated that the pyrolysis of *C. glomerata* is non-spontaneous toward biofuels production.

The ΔS parameter often denotes the degree of disorder involved in biomass conversion into biofuel via pyrolysis. The average values of ΔS for multi-stage analysis of *C. glomerata* pyrolysis were calculated as -29.01 ± 0.30 J mol⁻¹ K⁻¹ for the first stage, 62.13 ± 0.18 J mol⁻¹ K⁻¹ for the second stage, and -144.57 ± 0.21 J mol⁻¹ K⁻¹ for the third stage. Note that both negative and positive signs of ΔS confirm the high thermochemical complexity involved in *C. glomerata*

Table 4 Thermodynamic parameters with respect to the conversion degree estimated for each devolatilization stage during the pyrolysis of *C. glomerata*

Conversion	First stage			Second stage			Third stage		
	ΔH (kJ mol ⁻¹)	ΔG (kJ mol ⁻¹)	ΔS (J mol ⁻¹ K ⁻¹)	ΔH (kJ mol ⁻¹)	ΔG (kJ mol ⁻¹)	ΔS (J mol ⁻¹ K ⁻¹)	ΔH (kJ mol ⁻¹)	ΔG (kJ mol ⁻¹)	ΔS (J mol ⁻¹ K ⁻¹)
0.05	155.68	168.71	-28.36	217.96	180.88	62.34	150.39	268.00	-144.20
0.10	155.63	168.88	-28.46	217.95	180.82	62.33	150.36	268.56	-144.24
0.15	155.58	169.03	-28.56	217.94	180.75	62.31	150.32	269.12	-144.28
0.20	155.55	169.17	-28.64	217.93	180.69	62.30	150.29	269.67	-144.32
0.25	155.51	169.29	-28.71	217.92	180.63	62.28	150.26	270.23	-144.36
0.30	155.48	169.40	-28.78	217.92	180.57	62.27	150.23	270.76	-144.39
0.35	155.45	169.51	-28.84	217.91	180.51	62.26	150.20	271.29	-144.43
0.40	155.42	169.61	-28.90	217.90	180.46	62.25	150.17	271.82	-144.47
0.45	155.39	169.70	-28.96	217.89	180.40	62.23	150.14	272.33	-144.50
0.50	155.36	169.79	-29.01	217.89	180.34	62.22	150.11	272.82	-144.53
0.55	155.34	169.88	-29.06	217.88	180.29	62.21	150.08	273.30	-144.57
0.60	155.32	169.96	-29.10	217.87	180.23	62.19	150.06	273.77	-144.60
0.65	155.30	170.03	-29.15	217.86	180.17	62.18	150.03	274.22	-144.63
0.70	155.28	170.10	-29.19	217.86	180.12	62.17	150.00	274.66	-144.66
0.75	155.26	170.17	-29.22	217.85	180.07	62.16	149.98	275.08	-144.69
0.80	155.24	170.23	-29.26	217.84	180.01	62.15	149.96	275.49	-144.71
0.85	155.22	170.29	-29.29	217.83	179.96	62.14	149.93	275.87	-144.74
0.90	155.21	170.35	-29.32	217.83	179.91	62.12	149.91	276.24	-144.76
0.95	154.65	172.36	-30.34	216.65	171.24	60.39	149.03	291.70	-145.72
Average	155.36	169.81	-29.01	217.83	179.90	62.13	150.08	273.42	-144.57
±SD	0.15	0.53	0.30	0.12	0.91	0.18	0.18	3.13	0.21

pyrolysis, which is also a trend for thermodynamic studies on biomass pyrolysis [33, 52]. For ΔS values with a negative sign, the first and third pyrolysis stages tend to present a lower reactive characteristic. This is attributed to the fact that the degree of disorder of products formed by volatile release and molecular rearrangement was lower than that of the initial reactants, resulting in a more ordered state. The positive ΔS found in the second pyrolysis stage signifies a high reactive characteristic involved in pyrolysis reactions, indicating that an activated complex tends to be rapidly formed as a result of volatile release and molecular rearrangement [53]. From a thermodynamic point of view, negative ΔS values are interpreted as indicative of “slow” reactions, while positive ΔS values are considered as evidence of “fast” reactions [54]. Based on thermodynamic results, green macroalgae *C. glomerata* can be considered a viable alternative for bioenergy production.

4 Conclusions

This paper aimed to assess the bioenergy potential of *C. glomerata* based on the kinetic and thermodynamic parameters of pyrolysis. It was first assumed that the pyrolytic behavior of *C. glomerata* proceeds in the form of a three-step consecutive reaction. Isoconversional kinetic analysis revealed that average values of activation energy were in the range of 159.0–169.5, 221.4–239.3, and 156.4–168.3 kJ mol⁻¹ for the first, second, and third pyrolysis stages, respectively. According to the compensation effect method, pre-exponential factor values ranged from 3.65×10^7 to 3.65×10^{18} min⁻¹. The master plot method showed that the pyrolytic conversion of *C. glomerata* initiated by three-dimensional diffusion (D3) model with a transition to reaction order-based models (F3 and F1) at high temperatures. Finally, the overall kinetic expression (assuming three pyrolysis stages, i.e., the sum of three kinetic triplets) satisfactorily reproduced the experimental pyrolysis behavior (with $R^2 > 0.94$). From thermodynamic insights, the *C. glomerata* arises as a very prospective feedstock for bioenergy production. Our slow pyrolysis results provided useful information and confirmation that *C. glomerata* should be exploited for bioenergy and biochar on a commercial scale. The detailed kinetics and thermodynamics data presented here will be helpful in the design of a pyrolytic processing system for this and other related macroalgae.

Supplementary Information The online version contains supplementary material available at <https://doi.org/10.1007/s13399-022-02556-4>.

Author contribution Z.S collected the biomass and performed the TGA analysis under the supervision of A.I. and S.L.B. Then, S.L.B. performed other experiments and wrote the initial manuscript with Z.S.

The TGA data were analyzed by J.L.Z., and J.C.G. S., who extracted the kinetics and thermodynamics and refined the initial manuscript. A.I. edited the final version of the manuscript.

Funding We appreciate the funding and support of the Higher Education Commission of Pakistan. J. L. F. Alves gratefully acknowledges the postdoctoral fellowship from Brazil’s National Council for Scientific and Technological Development (CNPq – Process 152245/2020–0). J. C. G. da Silva gratefully acknowledges the grant from Brazil’s Coordination for the Improvement of Higher Education Personnel (CAPES – Finance Code 001).

Data availability Data will be provided upon request.

Declarations

Conflict of interest The authors declare no competing interests.

References

- Alves JLF, Da Silva JCG, da Silva Filho VF et al (2019) Bioenergy potential of red macroalgae *Gelidium floridanum* by pyrolysis: evaluation of kinetic triplet and thermodynamics parameters. *Bioresour Technol* 291:121892. <https://doi.org/10.1016/j.biortech.2019.121892>
- Arbeláez AA, Giraldo ND, Pérez JF, Atehortúa L (2019) Pyrolysis kinetics using TGA and simulation of gasification of the microalga *Botryococcus braunii*. *Bioenergy Res* 12:1077–1089. <https://doi.org/10.1007/s12155-019-10037-2>
- Lane DJ, Ashman PJ, Zevenhoven M et al (2014) Combustion behavior of algal biomass: carbon release, nitrogen release, and char reactivity. *Energy Fuels* 28:41–51. <https://doi.org/10.1021/ef4014983>
- Park KY, Lee K, Kim D (2018) Characterized hydrochar of algal biomass for producing solid fuel through hydrothermal carbonization. *Bioresour Technol* 258:119–124. <https://doi.org/10.1016/j.biortech.2018.03.003>
- Yao Z, Yu S, Su W et al (2020) Kinetic studies on the pyrolysis of plastic waste using a combination of model-fitting and model-free methods. *Waste Manag Res* 38:77–85. <https://doi.org/10.1177/0734242X19897814>
- Vasudev V, Ku X, Lin J (2020) Pyrolysis of algal biomass: determination of the kinetic triplet and thermodynamic analysis. *Bioresour Technol* 317:124007. <https://doi.org/10.1016/j.biortech.2020.124007>
- Anand V, Sunjeev V, Vinu R (2016) Catalytic fast pyrolysis of *Arthrospira platensis* (spirulina) algae using zeolites. *J Anal Appl Pyrolysis* 118:298–307. <https://doi.org/10.1016/j.jaap.2016.02.013>
- Ansah E, Wang L, Zhang B, Shahbazi A (2018) Catalytic pyrolysis of raw and hydrothermally carbonized *Chlamydomonas debararyana* microalgae for denitrogenation and production of aromatic hydrocarbons. *Fuel*. <https://doi.org/10.1016/j.fuel.2018.04.163>
- López-González D, Fernandez-Lopez M, Valverde JL, Sanchez-Silva L (2014) Pyrolysis of three different types of microalgae: kinetic and evolved gas analysis. *Energy*. <https://doi.org/10.1016/j.energy.2014.05.008>
- Zhao H, Yan HX, Liu M et al (2013) Production of bio-oil from fast pyrolysis of macroalgae *enteromorpha prolifera* powder in a free-fall reactor. *Energy Sources Part A Recover Util Environ Eff* 35:859–867. <https://doi.org/10.1080/15567036.2012.680000>

11. Salimi P, Norouzi O, Pourhosseini SEM et al (2019) Magnetic biochar obtained through catalytic pyrolysis of macroalgae: a promising anode material for Li-ion batteries. *Renew Energy*. <https://doi.org/10.1016/j.renene.2019.03.077>
12. Pourhosseini SEM, Norouzi O, Salimi P, Naderi HR (2018) Synthesis of a novel interconnected 3D pore network algal biochar constituting iron nanoparticles derived from a harmful marine biomass as high-performance asymmetric supercapacitor electrodes. *ACS Sustain Chem Eng*. <https://doi.org/10.1021/acssuschemeng.7b03871>
13. Michalak I, Baśladyńska S, Mokrzycki J, Rutkowski P (2019) Biochar from a freshwater macroalga as a potential biosorbent for wastewater treatment. *Water* 11:1390. <https://doi.org/10.3390/w11071390>
14. Mokrzycki J, Michalak I, Rutkowski P (2020) Biochars obtained from freshwater biomass—green macroalga and hornwort as Cr(III) ions sorbents. *Biomass Convers Biorefinery*. <https://doi.org/10.1007/s13399-020-00649-6>
15. Munir M, Qureshi R, Bibi M, Khan AM (2019) Pharmaceutical aptitude of *Cladophora*: a comprehensive review. *Algal Res* 39:101476. <https://doi.org/10.1016/j.algal.2019.101476>
16. Shahid A, Ishfaq M, Ahmad MS et al (2019) Bioenergy potential of the residual microalgal biomass produced in city wastewater assessed through pyrolysis, kinetics and thermodynamics study to design algal biorefinery. *Bioresour Technol* 289:121701. <https://doi.org/10.1016/j.biortech.2019.121701>
17. Plis A, Lasek J, Skawińska A, Zuwała J (2015) Thermochemical and kinetic analysis of the pyrolysis process in *Cladophora glomerata* algae. *J Anal Appl Pyrolysis* 115:166–174. <https://doi.org/10.1016/j.jaap.2015.07.013>
18. Norouzi O, Tavasoli A, Jafarian S, Esmailpour S (2017) Catalytic upgrading of bio-products derived from pyrolysis of red macroalgae *Gracilaria gracilis* with a promising novel micro/mesoporous catalyst. *Bioresour Technol* 243:1–8. <https://doi.org/10.1016/j.biortech.2017.06.072>
19. Ahmad MS, Liu CG, Nawaz M et al (2021) Elucidating the pyrolysis reaction mechanism of *Calotropis procera* and analysis of pyrolysis products to evaluate its potential for bioenergy and chemicals. *Bioresour Technol* 322. <https://doi.org/10.1016/j.biortech.2020.124545>
20. Vyazovkin S, Chrissafis K, Di Lorenzo ML et al (2014) ICTAC Kinetics Committee recommendations for collecting experimental thermal analysis data for kinetic computations. *Thermochim Acta* 590:1–23. <https://doi.org/10.1016/j.tca.2014.05.036>
21. Yao Z, Yu S, Su W et al (2020) Comparative study on the pyrolysis kinetics of polyurethane foam from waste refrigerators. *Waste Manag Res* 38:271–278. <https://doi.org/10.1177/0734242X19877682>
22. Qi W, Yang W, Xu Q et al (2020) Comprehensive research on the influence of nonlignocellulosic components on the pyrolysis behavior of Chinese distiller's grain. *ACS Sustain Chem Eng* 8:3103–3113. <https://doi.org/10.1021/acssuschemeng.9b05848>
23. Yao Z, Xiong J, Yu S et al (2020) Kinetic study on the slow pyrolysis of nonmetal fraction of waste printed circuit boards (NMF-WPCBs). *Waste Manag Res* 38:903–910. <https://doi.org/10.1177/0734242X19896630>
24. Alves JLF, da Silva JCG, Languer MP et al (2020) Assessing the bioenergy potential of high-ash anaerobic sewage sludge using pyrolysis kinetics and thermodynamics to design a sustainable integrated biorefinery. *Biomass Convers Biorefinery*. <https://doi.org/10.1007/s13399-020-01023-2>
25. Peña JAT, Pacheco LCA, Tovar LP, Franco TT (2021) Non-isothermal decomposition kinetics of lipids recovered from oleaginous microbial biomass (*C. vulgaris* and *L. starkeyi*): reaction mechanism and TGA-MS analysis. *BioEnergy Res*. <https://doi.org/10.1007/s12155-021-10271-7>
26. Vyazovkin S, Burnham AK, Criado JM et al (2011) ICTAC Kinetics Committee recommendations for performing kinetic computations on thermal analysis data. *Thermochim Acta* 520:1–19. <https://doi.org/10.1016/j.tca.2011.03.034>
27. Starink MJ (2003) The determination of activation energy from linear heating rate experiments: a comparison of the accuracy of isoconversion methods. *Thermochim Acta* 404:163–176. [https://doi.org/10.1016/S0040-6031\(03\)00144-8](https://doi.org/10.1016/S0040-6031(03)00144-8)
28. Alves JLF, da Silva JCG, Mumbach GD et al (2022) Prospection of catole coconut (*Syagrus cearensis*) as a new bioenergy feedstock: insights from physicochemical characterization, pyrolysis kinetics, and thermodynamics parameters. *Renew Energy* 181:207–218. <https://doi.org/10.1016/j.renene.2021.09.053>
29. Mumbach GD, Alves JLF, da Silva JCG et al (2022) Prospecting pecan nutshell pyrolysis as a source of bioenergy and bio-based chemicals using multicomponent kinetic modeling, thermodynamic parameters estimation, and Py-GC/MS analysis. *Renew Sustain Energy Rev* 153:1–13. <https://doi.org/10.1016/j.rser.2021.111753>
30. Alves JLF, da Silva JCG, Mumbach GD et al (2022) Potential of macauba endocarp (*Acrocomia aculeate*) for bioenergy production: multi-component kinetic study and estimation of thermodynamic parameters of activation. *Thermochim Acta* 708:179134. <https://doi.org/10.1016/j.tca.2021.179134>
31. Alves JLF, da Silva JCG, Mumbach GD et al (2020) Thermo-kinetic investigation of the multi-step pyrolysis of smoked cigarette butts towards its energy recovery potential. *Biomass Convers Biorefinery*. <https://doi.org/10.1007/s13399-020-01077-2>
32. Fernandez A, Ortiz LR, Asensio D et al (2020) Kinetic analysis and thermodynamics properties of air/steam gasification of agricultural waste. *J Environ Chem Eng* 8:103829. <https://doi.org/10.1016/j.jece.2020.103829>
33. Gupta S, Gupta GK, Mondal MK (2020) Thermal degradation characteristics, kinetics, thermodynamic, and reaction mechanism analysis of pistachio shell pyrolysis for its bioenergy potential. *Biomass Convers Biorefinery* 10:1–15. <https://doi.org/10.1007/s13399-020-01104-2>
34. Maia AAD, de Moraes LC (2016) Kinetic parameters of red pepper waste as biomass to solid biofuel. *Bioresour Technol* 204:157–163. <https://doi.org/10.1016/j.biortech.2015.12.055>
35. Xu X, Chen R, Pan R, Zhang D (2020) Pyrolysis kinetics, thermodynamics, and volatiles of representative pine wood with thermogravimetry–Fourier transform infrared analysis. *Energy Fuels* 34:1859–1869. <https://doi.org/10.1021/acs.energyfuels.9b03872>
36. Gao W, Chen K, Zeng J et al (2017) Thermal pyrolysis characteristics of macroalgae *Cladophora glomerata*. *Bioresour Technol* 243:212–217. <https://doi.org/10.1016/j.biortech.2017.06.041>
37. Norouzi O, Jafarian S, Safari F et al (2016) Promotion of hydrogen-rich gas and phenolic-rich bio-oil production from green macroalgae *Cladophora glomerata* via pyrolysis over its bio-char. *Bioresour Technol* 219:643–651. <https://doi.org/10.1016/j.biortech.2016.08.017>
38. Badshah SL, Shah Z, Francisco Alves JL et al (2021) Pyrolysis of the freshwater macroalgae *Spirogyra crassa*: evaluating its bioenergy potential using kinetic triplet and thermodynamic parameters. *Renew Energy* 179:1169–1178. <https://doi.org/10.1016/j.renene.2021.07.105>
39. Kim SS, Ly HV, Kim J et al (2013) Thermogravimetric characteristics and pyrolysis kinetics of *Alga Sagarssum* sp. biomass. *Bioresour Technol* 139:242–248. <https://doi.org/10.1016/j.biortech.2013.03.192>
40. Das P, Mondal D, Maiti S (2017) Thermochemical conversion pathways of *Kappaphycus alvarezii* granules through study of kinetic models. *Bioresour Technol* 234:233–242. <https://doi.org/10.1016/j.biortech.2017.03.007>

41. Müsellim E, Tahir MH, Ahmad MS, Ceylan S (2018) Thermokinetic and TG/DSC-FTIR study of pea waste biomass pyrolysis. *Appl Therm Eng* 137:54–61. <https://doi.org/10.1016/j.applthermaleng.2018.03.050>
42. Gözke G, Açıkalın K (2020) Pyrolysis characteristics and kinetics of sour cherry stalk and flesh via thermogravimetric analysis using isoconversional methods. *J Therm Anal Calorim*. <https://doi.org/10.1007/s10973-020-10055-9>
43. Moine Ec, Groune K, El Hamidi A et al (2016) Multistep process kinetics of the non-isothermal pyrolysis of Moroccan Rif oil shale. *Energy* 115:931–941. <https://doi.org/10.1016/j.energy.2016.09.033>
44. Bhagavatula A, Shah N, Honaker R (2016) Estimating the pyrolysis kinetic parameters of coal, biomass, and their blends: a comparative study. *Energy Fuels* 30:10045–10054. <https://doi.org/10.1021/acs.energyfuels.5b00692>
45. Pinzi S, Buratti C, Bartocci P et al (2020) A simplified method for kinetic modeling of coffee silver skin pyrolysis by coupling pseudo-components peaks deconvolution analysis and model free- isoconversional methods. *Fuel* 278:118260. <https://doi.org/10.1016/j.fuel.2020.118260>
46. da Silva JCG, de Albuquerque JG, de Galdino WV, A et al (2020) Single-step and multi-step thermokinetic study – deconvolution method as a simple pathway for describe properly the biomass pyrolysis for energy conversion. *Energy Convers Manag* 209:112653. <https://doi.org/10.1016/j.enconman.2020.112653>
47. Kaur R, Gera P, Jha MK, Bhaskar T (2018) Pyrolysis kinetics and thermodynamic parameters of castor (*Ricinus communis*) residue using thermogravimetric analysis. *Bioresour Technol* 250:422–428. <https://doi.org/10.1016/j.biortech.2017.11.077>
48. Vyazovkin S, Burnham AK, Favergeon L et al (2020) ICTAC Kinetics Committee recommendations for analysis of multi-step kinetics. *Thermochim Acta* 689:178597. <https://doi.org/10.1016/j.tca.2020.178597>
49. Konwar K, Nath HP, Bhuyan N et al (2019) Effect of biomass addition on the devolatilization kinetics, mechanisms and thermodynamics of a northeast Indian low rank sub-bituminous coal. *Fuel* 256:115926. <https://doi.org/10.1016/j.fuel.2019.115926>
50. Alves JLF, Da Silva JCG, Di Domenico M et al (2020) Exploring Açai seed (*Euterpe oleracea*) pyrolysis using multi-component kinetics and thermodynamics assessment towards its bioenergy potential. *Bioenergy Res* 14:209–225. <https://doi.org/10.1007/s12155-020-10175-y>
51. Aslan DI, Özoğul B, Ceylan S, Geyikçi F (2018) Thermokinetic analysis and product characterization of medium density fiberboard pyrolysis. *Bioresour Technol* 258:105–110. <https://doi.org/10.1016/j.biortech.2018.02.126>
52. Tahir MH, Çakman G, Goldfarb JL et al (2019) Demonstrating the suitability of canola residue biomass to biofuel conversion via pyrolysis through reaction kinetics, thermodynamics and evolved gas analyses. *Bioresour Technol* 279:67–73. <https://doi.org/10.1016/j.biortech.2019.01.106>
53. Mumbach GD, Alves JLF, da Silva JCG et al (2020) Pyrolysis of cocoa shell and its bioenergy potential: evaluating the kinetic triplet, thermodynamic parameters, and evolved gas analysis using TGA-FTIR. *Biomass Convers Biorefinery*. <https://doi.org/10.1007/s13399-020-01058-5>
54. Boonchom B, Puttawong S (2010) Thermodynamics and kinetics of the dehydration reaction of FePO₄·2H₂O. *Phys B Condens Matter* 405:2350–2355. <https://doi.org/10.1016/j.physb.2010.02.046>

Publisher's note Springer Nature remains neutral with regard to jurisdictional claims in published maps and institutional affiliations.